

Haptic Augmentation Towards a Smart Learning Environment: The Haptic Lever Design

ALMA GUADALUPE RODRÍGUEZ RAMÍREZ¹, MANUEL NANDAYAPA¹, (Member, IEEE),
OSSLAN OSIRIS VERGARA VILLEGAS¹, (Senior Member, IEEE) and FRANCESCO GARCÍA
LUNA¹

¹Universidad Autónoma de Ciudad Juárez, Avenida del Charro 450 Norte, Partido Romero 32310, Juárez, Chihuahua, México. (e-mail: alma.rodriguez.ram@uacj.mx, mnandaya@uacj.mx, overgara@uacj.mx, francesco.garcia@uacj.mx)

Corresponding author: Alma Rodríguez (e-mail: alma.rodriguez.ram@uacj.mx).

ABSTRACT This paper presents the design of a haptic interface called the Haptic Lever, to show four force-related phenomena for haptic augmentation towards Smart Learning Environments. The Haptic Lever is a mechanism with a sensorless torque control developed by means of a Disturbance Observer (DOB) to render forces that allow users to feel virtual phenomena. The control response converges in the torque reference as a result of a gain calibration and the DOB response. The Haptic Lever was evaluated experimentally with four dynamic models for constant (membrane), linear (Hook's law and viscous damping), and exponential (Coulomb's law) haptic augmentation. In the first experiment, the user can feel a constant force when passing between two reference points and feel resistance while moving through a virtual membrane. In the second and third experiment, the user can feel and interact with the linear dynamic models of Hook's law and viscous damping, in the form of a compression or tension spring by pushing or pulling them, respectively. Finally, in the fourth experiment, the user can feel an attraction or repulsion force between two virtual point charges that follows the exponential dynamic model of Coulomb's law. The results obtained from the experiments showed that the Haptic Lever successfully rendered the equivalent forces to each virtual phenomenon. The haptic sensation is estimated in terms of the torque response under a profile determined by the dynamic models. From the experimental results, it can be observed that the torque in Nm corresponded to each represented phenomenon.

INDEX TERMS disturbance observer, haptic augmentation, haptic lever, sensorless torque control, smart learning environment

I. INTRODUCTION

TRADITIONALLY, students learn in an environment where all the theoretical information is offered by the teacher. The common senses used in traditional learning environments are sight and hearing, leaving aside one of the most important senses when it comes to interaction with an environment, the sense of touch (haptic feedback). There are different kinds of learners classified by how they prefer to acquire knowledge e.g. visual, or auditory, kinesthetic (VAK). Visual learners retain information better when it is presented with pictures or diagrams. Auditory learners prefer to hear what is being presented. On the other hand, kinesthetic learners are those who understand things easily when learning involves movements and touch (hands-on activities). According to [1], most people remember kinesthetic skills

better and longer than verbal or visual, which confirms the importance of integrating haptic feedback in the learning process. Moreover, visual and auditory learners may also improve their learning through haptics [2]. According to the cone of learning proposed by Edgar Dale in 1969, people retain about 90% of what they do and say (active learning). Active learning can be carried out through real or simulated experiences [3].

Different studies have investigated the integration of haptic sensations in the learning process [4]–[15]. One of them proposes the use of tangible user interfaces (TUI) in which the student interacts with virtual and real objects at the same time [16]. TUIs integrate haptic feedback in virtual interactions through real objects. Another alternative is the use of augmented reality (AR) techniques like SoftAR [17],

where a deformation is projected in a real object as a visual-haptic effect, making it appear deformed even though the student does not experience an actual haptic feedback. In this paper, haptic augmentation is presented as an alternative to traditional and passive learning approaches, for interacting with abstract topics such as physical phenomena.

The haptic interaction that students have with theoretical information may be enhanced with interactive technology [4], [5]. Haptic interactive technology may facilitate hands-on laboratory content by improving learning in topics like physics [4], chemistry [6], mechatronics [7], mechanics [8], [9], electricity and magnetism [10], mathematics [11], manufacture [12], [13], and medicine [14], [15]. The need for alternative tools and methods that increase learning outcomes has driven many investigations towards enhanced learning e.g. flipped classrooms [18], smart classrooms [19], eLearning [20], game-based learning [21], [22], and virtual learning environments [6], [23], where interactive activities are fundamental. The introduction of the term “smart learning” enrolls a context where scientists have tried to solve the problem of how to integrate technology and interactivity in the classroom to enhance learning outcomes as well as teaching.

The International Association of Smart Learning Environments (IASLE) has defined it as: “an emerging area of challenging exploitation of smart environments for learning, together with new technologies and approaches such as ubiquitous learning and mobile learning” [24]. Rob Koper in [25] defined a set of requirements for Smart Learning Environments (SLEs) based on a digital case and a side-by-side case where the learning solutions could be computer-based, focusing on the addition of digital devices that augment and facilitate information, collaboration, monitoring and context, among others. The Haptic Lever, as a technological learning solution for SLEs, satisfies the requirement of augmenting the information given to the student as proposed by Rob Koper in [25].

Technological tools may help in precise interventions in learning environments by increasing student motivation, creative thinking, and engagement [4], [23], [26]. There are many approaches towards SLEs and smart classrooms, such as evaluation and development frameworks [27], [28], activity assessment development [19], organizational tools [29], and incorporation of interactive technological tools [25]. In this paper, the last approach was adopted to create SLEs, by generating a haptic sensation upon interaction with physical phenomena through an interface.

Physical phenomena were chosen for testing the Haptic Lever because full understanding and comprehension of physical phenomena require more than theoretical concepts. Haptic augmentation may lead students to a better conception of invisible phenomena in the physical sciences [30]. Therefore, physics is a subject with potential for the integration of haptic feedback in the learning process. Physical interaction becomes essential to comprehend abstract topics in learning situations. Some of the most common physics topics that students must comprehend are simple machines, displacement,

force and motion, momentum, collisions, work and energy, thermodynamics, and electric force. A kinesthetic haptic interface could represent any of these topics/phenomena experimentally. There is a need for alternative interactive tools that are capable of displaying forces and, therefore, can represent physical phenomena so the students may interact with them experimentally.

Although the importance of haptic feedback in education has been studied for a long time, there is still an opportunity for haptics in future educational areas like SLEs. The Haptic Lever is presented as an alternative didactic tool that can display forces and, therefore, represent many abstract topics related to force interaction. This research could benefit education in the future by easing the knowledge building and understanding of physical phenomena as well as the introduction and development of haptic interfaces at different educational levels. In this paper, the Haptic Lever is presented as a device that generates a realistic haptic feedback due to the DOB-based sensorless torque control design. For the control scheme, the use of experimental motor parameters leading to a low parameter variation and the control gains tuning based on open and closed loop calibrations are proposed. All the algorithms were implemented in a Field-Programmable Gate Array (FPGA) because it offers parallel processing, multi-clock applications, high-speed operation, and flexible hardware configuration. The design is based on a simple machine (lever) since it can represent many interactive situations like the sensation of abdominal palpation during diagnosis [31], changing a car turn-switch signal [32], controlling the throttle of an aircraft [33], or experimenting specific physical phenomena.

The Haptic Lever was tested using four physics experiments considering constant (membrane), linear (Hooke's Law and viscous damping), and exponential force (Coulomb's Law) behavior. The student or teacher can experience any of the four virtual phenomena by grasping the lever with the hand and manipulating its position. Depending on the user's motion, the Haptic Lever displays the force corresponding to the experiment selected.

The rest of the paper is organized as follows. Section II describes different haptic interfaces, and their characteristics. Section III presents the methodology followed to develop the Haptic Lever. In section IV, the experimental results of the implementation of the Haptic Lever for constant, linear, and exponential haptic augmentation are presented by representing a virtual membrane, a virtual spring, and virtual point charges. Finally, conclusions are presented in Section V.

II. INTERFACES FOR HAPTIC AUGMENTATION

A haptic interface can be designed with cutaneous and/or kinesthetic feedback. The cutaneous feedback is related to textures and vibration, while the kinesthetic is related to motion and force reaction. Humans interact with the world through both types, but there are technical difficulties for the development of haptic devices that integrate both types of feedback. The development of haptic-enabled environ-

ments is quite challenging when it comes to mechanical design, actuators, real-time systems, rendering algorithms, user-object interaction modeling, human capabilities, and other areas [34]. This section describes non-commercial interfaces developed to perform haptic augmentation through cutaneous, kinesthetic or both types of haptic feedback. Most of the works presented in this section foresee applications for educational purposes.

One approach to the design of haptic interfaces is to include both kinesthetic and cutaneous haptic feedback. Whitmire et al. [35] developed a re-configurable haptic revolver to enable the feeling of touch in the index fingertip. The cutaneous feedback represented texture with different wheel materials while the kinesthetic feedback consisted of rotating and moving the wheel towards the finger for representing the breaking contact with a surface. Son and Park designed an interface in the form of a glove [36] for the manipulation of variable size virtual objects with kinesthetic feedback on the fingers and cutaneous feedback on palm and fingers. Chinello et al. presented a wearable finger interface with a kinesthetic and a cutaneous module [37]. The device consisted of a 3 degrees of freedom (DoF) platform that got in contact with the fingertip for combined feedback. Lee et al. [38] used the motion of micro actuators to generate feedback forces augmentation over the fingertip when interacting with a virtual object (e.g. squeezing). In most approaches of combined feedback, the kinesthetic feedback was limited in space and force magnitude in comparison to fully kinesthetic interfaces. To overcome this limitation, other works have presented combined feedback by integrating cutaneous haptic devices with commercial kinesthetic devices [39]–[41].

Cutaneous feedback is usually represented by a magnetic field [42], vibration and thermal feedback [43], [44], and skin stretch [45], [46]. The cutaneous haptic feedback based on a magnetic field, still needs to deal with magnetic interference when performing multiple direction feedback. Moreover, vibration and thermal feedback can be presented in a variety of patterns, but the synchronization in multimodal applications is an important issue. As an alternative or supportive feature to vibration stimuli, skin stretch performs haptic augmentation by skin deformation.

Kinesthetic haptic interfaces are mainly related to position and force feedback. Many investigations have been made to overcome the limitations of workspace [47], stationary operations [48], and high cost [7], among others. Tong et al. [47] proposed magnetic levitation haptic augmentation for the perception of virtual tissue stiffness. The haptic device controlled a coil current generating a desired magnetic field. Grajewski et al. [48] enabled a virtual workplace with haptic feedback for manufacturing tasks. Okamura et al. [7] developed a low-cost haptic joystick called the haptic paddle as a laboratory tool for dynamic systems, modeling, and control courses. The haptic paddle has driven other research related to educational applications [8], [9], [49]–[51] due to its flexibility for representing physical interactions.

The design of kinesthetic haptic devices tends to simulate

a large variety of tasks, to emulate a force reaction, or to augment an applied force in a task. Other devices have more complex mechanisms for representing more than one task. Choi et al. [52] developed CLAW, a handheld haptic controller for grasping, touching, and triggering in virtual reality. Zhao et al. [53] developed Canetroller, a haptic cane with auditory feedback. The haptic cane enables people with visual impairments to navigate virtual reality environments. Strasnick et al. [54] designed the Haptic Links which are a set of haptic devices electro-mechanically actuated. designed the Haptic Links, a set of electro-mechanically actuated haptic devices. The devices could render variable stiffness between two handheld VR controllers. Ando et al. [55] develop a haptic interface called Force Blinker 2 for navigation. The device allows the user to recognize four traveling directions through centrifugal force generated on a rail with a motor, a movable weight, a movable magnet and a fixed magnet. Lee et al. [56] developed a Hand-Held Force Magnifier as a robotic surgical instrument. The user can feel a magnified contact force, generated in a contact task, through the needle-type interface.

Table 1 presents a brief description of haptic interfaces designed to perform haptic augmentation with different approaches. A general description of each device's design is provided in the second column while the number of DoFs are shown in the third column. The DoFs are variable and depend on the haptic rendering representations the interfaces were designed to perform. Since the DoF is a characteristic that relates to a mechanism and its movements, the DoF of the vibratory interfaces was determined by the direction effect felt by the user due to the vibration. Like the Haptic Lever, many interfaces were done with only one DoF, but it does not entirely limit the number of situations that a haptic device can represent. In the fourth column, the control schemes are presented. The classic control schemes (Proportional (P), Proportional Derivative (PD), Proportional Integral (PI), Proportional Integral Derivative (PID)) are the most common schemes implemented. Meanwhile, the Haptic Lever proposes a DOB-based control designed with experimental parameters and a gain calibration method. The DOB has proven to be a good alternative to the classic control schemes in motion control [57]–[59] as well as to the use of force sensors. The controller board is crucial in the development of haptic devices since its processing capacity impacts directly on the performance. As can be observed from column six, unlike our work none of the works discussed implemented their algorithms in an FPGA, although it offers parallel processing, multi-clock applications, high-speed operation, real-time processing, re-programmability and a flexible hardware configuration. FPGAs have been widely used by other works related to haptic feedback in teleoperation [60], [61] and force/torque control [62]. Haptic systems are closely related to teleoperated systems due to their bilateral nature in which the stability and good transparency performance are the main challenges. Chen et al. faced those challenges with an adaptive fuzzy backstepping control [63] while we

TABLE 1. A summary of the characteristics of 18 custom-designed haptic interfaces

Author	Haptic interface	DoF	Control scheme	Force sensor	Controller board	Force capacity	Wearable	Haptic augmentation
<i>Cutaneous and kinesthetic feedback</i>								
Whitmire et al. [35]	Wheel and trigger	2	PID	No	Cypress PSoc SLP	Up to 3,35N	No	Touch contact, pressure, shear force, textures and shapes
Son and Park [36]	Glove	3/1	P	No	Atmega328 / Motor driver	Object stiffness 0.2 - 0.5N/m	Yes	Sphere of different sizes
Chinello et al. [37]	Finger	3/1	PID	No	-	-	Yes	Curvature discrimination, tumor palpation, and virtual object grasping
Lee et al. [38]	Hand-held controller	1	P	Yes	Teensy 3.6	Applied 170Hz vibration per 0.49N	Yes	Squeezing, shearing, and turning tasks performed by grasping/releasing, compliance and texture in-hand exploration, and manipulation of a virtual object
<i>Cutaneous feedback</i>								
Kim et al. [42]	Fingertip	3	Analog PD	No	Arduino Due	-	Yes	2D Tangential forces and 1D normal force
G. Park et al. [43]	Ring/Box	1	Preset pattern	No	NUCLEO-F334R8; Mbed	-	Yes	Gaming, haptic functionality to ordinary objects, identification of contact and location patterns
García-Valle et al. [44]	Vest	1	Preset pattern	No	Arduino Lilypad / PCB Power Stage	-	Yes	Collision (at low or high velocity) and temperature simulation (stress, physical activity, and closeness to fire)
F. Chinello et al. [45]	Bracelet	2	P	No	Raspberry Pi Model B and Arduino Mini	-	Yes	Provides navigation information related to pronation, supination, and translation for rotating, translating, grasping or lifting a target
Culbertson et al. [46]	Finger attachments	3	Preset pulses	No	Sensoray 826 PCI card	-	Yes	Direction cues of translation (left, right, forward, backward, up, down) and rotation (radial deviation, ulnar deviation, extension, flexion, pronation, supination)
<i>Kinesthetic feedback</i>								
Okamura et al. [7]	Paddle	1	PD	No	CIO-DAS1600 / CIO-DDA06	Up to 7.5N approx.	No	Variety of virtual dynamic systems
Tong et al. [47]	Magnetic levitation	-	Self - adaptative PID	No	ARM Cortex-M MCU	Up to 2N	No	Virtual tissue stiffness
Grawjewski et al. [48]	Delta robot	3	-	No	-	-	No	Virtual objects like a wall or a table
Choi et al. [52]	Hand-held controller	7	PD / admittance	Yes	Teensy 3.3	Up to 30N	Yes	Kinesthetic feedback for grasping, touching, and triggering and vibration normal to fingertip for textures
Zhao et al. [53]	Cane	1	Play recorded data	No	Pololu 18v7-break Pololu miniMU-9 v5-vibrations	Break percentage	Yes	Virtual wall with shore-lining, two-point touch, constant contact, and penetration into a virtual wall
Strasnick et al. [54]	Bi-manual hand-held control	2	-	No	Teensy 3.2	Chain and Lever hinge - 1.1Nm Ratchet hinge - 0.7Nm	No	Rifle, bow, trombone, and pistols
Ando et al. [55]	Rail with movable weight/magnet	1	Passive	No	H8/3052F	1.3N	No	Navigation with recognition of traveling direction (forward, backward, left, and right) by the visually impaired
Lee et al. [56]	Needle	1	P	Yes	ADuC7026	Up to 0.86N	No	Force matching, minimum contact
Our work	Lever	1	DOB-based control with gain calibration	No	Altera DE0-Nano FPGA	-0.5Nm to 0.5Nm	No	Virtual membranes/barriers, springs, and point charges.

propose taking the advantages of an FPGA before mentioned. The force capacities varied among devices since they depend on the task the device was designed to perform. From the eighth column, it can be observed that most interfaces with cutaneous and combined feedback are wearable. Wearability provides mobility, which is an important issue in interactive activities so there is a tendency to design wearable and multi-task haptic devices. In the last column, a summary of the haptic augmentation performed by each interface is presented. Certainly, all works have potential to perform more tasks, but only the tasks tested in each research are presented. There are opportunities in the future for further development of the Haptic Lever in terms of combined feedback, wearability, and multi-task applications.

III. THE HAPTIC LEVER

In the proposed method for the development of the Haptic Lever, there is no need for a force/torque sensor since the control is based on a DOB. The motor shaft works as the lever's pivot and the force/torque generator. The complete development of the Haptic Lever was made in three stages: The Haptic Lever design, the angular velocity estimation, and the DOB design.

In the first stage, the design and configuration of the interface are shown, they are based on a simple implementation. The second and third stages are related to the sensorless torque control required to render forces. In the second stage, the implementation of the N-method for the velocity estimation is described. In the third stage, the DOB-based sensorless torque control design is presented.

The device generates a realistic haptic feedback due to

the DOB-based sensorless torque control design. The control scheme has a low parameter variation because of the estimation of the experimental parameters instead of the nominal values commonly used in DOB-based controls. The control gains were tuned using open and closed loop calibrations. The calibrations ensure that the DOB response is close to the real torque exerted by the device.

A. THE HAPTIC LEVER DESIGN

The Haptic Lever was designed as a one DoF system for basic implementation of haptic augmentation with the objective of being a startup point for the development of an SLE. The Haptic Lever can display interaction forces that occur when humans interact with different objects like membranes, springs, and charged particles.

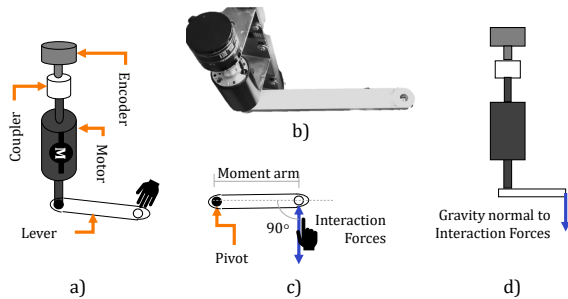


FIGURE 1. The Haptic Lever: a) The Haptic Lever diagram and parts b) Real representation of the Haptic Lever c) Force interaction considerations d) Gravity force consideration

The Haptic Lever is a human-machine interface (HMI) that allows the user to have the feeling of interacting with different objects through touch (see Figure 1b). Since the lever is directly joined to the motor's shaft (see Figure 1a), the output torque of the Haptic Lever is proportional to the moment arm and the force applied (see equation (1)). The motor is vertically positioned so that the force applied at the end of the lever is normal to the gravitational force, implying that the gravity does not affect the interaction between the user and the machine (see Figure 1d). The interaction forces are considered tangential from the pivot of the lever, meaning that there are ninety degrees between the moment arm and the interaction forces (see Figure 1c). In this case, the motor shaft works as the pivot of the lever. The interaction forces are the forces that the user applies to interact with the Haptic Lever and the force exerted by the motor.

$$\tau_{out} = Fr \quad (1)$$

where τ_{out} is the output torque executed by the motor, F is the force applied at the end of the lever, and r is the moment arm.

The final design of the Haptic Lever is depicted in Figure 2. The mechanism includes a 24V DC motor (MAXON 148867) instrumented with an incremental quadrature encoder (YUMO E6B2-CWZ3E). The controller board is a

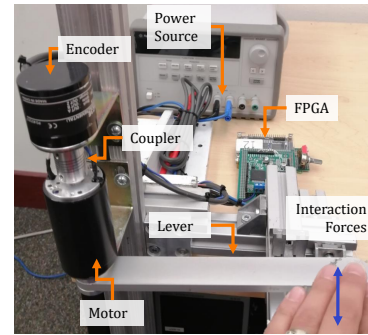


FIGURE 2. The Haptic Lever.

DE0-Nano Altera Cyclone IV FPGA that runs at 50 MHz, enabled with multi-clock applications (up to 20 different clocks). The haptic rendering, which is the computed torque, is programmed by means of a sensorless torque control based on DOB.

The DOB allows the user to feel the torque applied by the motor in the form of a force. The force displayed in the Haptic Lever can go from -0.5 Nm to 0.5 Nm due to the 7A of current that the power source can deliver. The control has the advantage that no force or torque sensor is required, although two calibrations are made to adjust the proportional control gains. The lever is positioned on the motor shaft, and its length is taken as the moment arm. When computing the torque applied, the interaction forces are assumed to be normal to the moment arm. The motor has an aluminum base set in a vertical position to avoid the addition of gravitational force to the interaction force in the lever.

B. ANGULAR VELOCITY ESTIMATION WITH N-METHOD

Once the Haptic Lever was built, the next stage was the estimation of the angular velocity. It is important to estimate the angular velocity estimation to achieve a good performance of the sensorless torque control presented in this paper. The control is based on a DOB that determines the torque response corresponding, mainly, to the motor's velocity, inertia, and torque constant. If the angular velocity estimation method is not appropriate, the control may not work properly. The encoder used for the development of the Haptic Lever was incremental. As shown in Figure 3, A and B channels of the encoder should be connected to a logical level converter (3.3V to 5V) if the controller board has a different logic level. The channels are then connected to the pins of the controller's General-Purpose Input/Output (GPIO) header. The channels are read by the FPGA and codified in the processor by a quadrature encoder block; as a result, this block gives the direction of the motors motion and four pulses per increment since the block algorithm check for every change in the channels levels.

The system feedback is the angular velocity $\hat{\omega}$ in rad/s, estimated with the N-method proposed by Nandayapa et al. [64]. The N-method, unlike the widely used M-method, is used for short sampling time and fast clock signal appli-

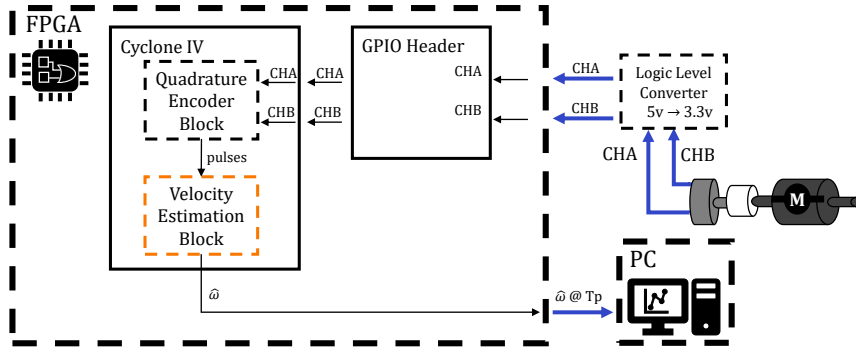


FIGURE 3. Experimental setup for the angular velocity estimation.

cations. Since the Haptic Lever considers an FPGA as the controller board, the N-method suits the velocity estimation.

The N-method was used in a discrete domain as in [64], with equation (2).

$$G_{\hat{\theta}}(z) = (1 - z^{-m_1})(2^n) \frac{a_1}{1 - b_1 z^{-1}} \quad (2)$$

where a_1 and b_1 are the low pass filter (LPF) coefficients estimated with the cut-off frequency, 2^n is a factor of the N-method to reduce the computational complexity of the velocity estimation whose value depends on the encoder resolution E_r , and m_1 is the number of samples required in the processing time T_p between the current $\theta(k)$ and previous position $\theta(k - m_1)$ for estimating $\hat{\omega}$, being k the current time when the sample z is read.

The incremental encoder is a YUMO E6B2-CWZ3E with a resolution of 1024 pulses per revolution. The quadrature encoder block runs at 50 MHz and counts at every change in the channels' level multiplying the encoder's resolution by four. The angular velocity estimation block is implemented at 1 MHz; therefore, T_p is considered a short sampling time, required for the implementation of the N-method.

A high frequency for processing the angular velocity estimation block increases the estimation accuracy. The accuracy is due to the many velocity calculations made in the single sampling time used in the M-method or other derivation techniques. The designer must consider the recommendation offered in [65], where the product of T_p and m_1 should be around $100 \mu s$ based on functional PC-based applications. The experimental parameters for the angular velocity estimation are depicted in Table 2.

TABLE 2. Experimental parameters for the angular velocity estimation

Parameter	Value
E_r	4096
T_p	1×10^{-6}
m_1	386
n	2

After the estimation of the angular velocity, the data goes through an LPF with a cut-off frequency of $\omega_c = 500$ rad/s,

selected experimentally. ω_c should be as high as possible, as long as it does not interfere with the estimation of the angular velocity. The cut-off frequency of the angular velocity estimation and the cut-off frequency of the DOB should have the same value since the DOB response depends on the velocity estimated. For example, if the cut-off frequency of the velocity estimation is higher than the DOB's, the DOB will not be able to see some of the frequencies from the velocity data. The cut-off frequency should be a high value allowing the DOB to identify high frequency disturbances.

C. DOB DESIGN

In general, an observer is a technique where the model of the plant is used for estimating variables that cannot be measured directly; therefore, the values are estimated from the known parameters and measurable variables. The Haptic Lever's control was designed based on a DOB, presented by Professor Ohnishi in 1983 [66]. The general concept of the DOB was to estimate a load torque with the system's known parameters and use it to compensate the system by canceling the effects of any external disturbance. Other techniques require complex algorithms and a large number of operations in comparison to the DOB. Although there are other techniques (e.g., Sliding Mode Control (SMC) [67]) proposed in the robust control field to improve the stability and performance of the control system in dealing with different disturbances and uncertainties, the DOB technique is one of the most popular due to its simplicity, flexibility, and efficacy [68]. Other disturbance/uncertainties estimation techniques are discussed and compared in [69].

The implementation of a DOB allows the design of a sensorless torque control and compensation of lumped disturbances. The torque applied by the motor is estimated as a disturbance/load torque with the torque constant K_t , motor's current I_a , motor's inertia J , and the second time derivative of the position $\ddot{\theta}$.

The dynamic model of the DC motor considered is the one from equation (3).

$$J\ddot{\theta} = K_t I_a - \tau_i - \tau_e - \tau_f - \tau_{reac} \quad (3)$$

where $\ddot{\theta}$ is the angular acceleration, I_a is the torque current, τ_i is the interactive torque that includes the Coriolis and gravitational terms, τ_e is the reaction torque of the motor when working. Finally, τ_f is the torque related to the viscous and Coulomb friction while τ_{reac} is the reaction torque caused by an external torque.

The negative torques in the model reduce the output torque ($J\ddot{\theta}$ term), they are all taken as a disturbance leading to the simplified model depicted in equation (4).

$$J\ddot{\theta} = K_t I_a - \tau_{dis} \quad (4)$$

where τ_{dis} is the disturbance torque.

The basic form of the DOB method is shown in Figure 4. Given an armature current of reference, the motor moves at a certain rate of acceleration or velocity determined by the total inertia J , the torque constant K_t , and a torque load τ_{load} . The τ_{load} is the external torque load that represents external disturbances (τ_{dis}), and $\hat{\tau}_{dis}$ is the disturbance torque observed by the DOB. The same armature current reference enters the DOB to estimate $\hat{\tau}_{dis}$ based on the nominal torque constant K_{tn} , the velocity response $\dot{\theta}$, the nominal inertia J_n , and an LPF. The g_{dis} is the cut-off frequency of an LPF that sets the bandwidth of the DOB. Since g_{dis} is the upper limit of the bandwidth, the DOB rejects any disturbances exceeding this limit. Therefore, the g_{dis} should be as high as possible, as long as it does not affect the system stability. The method also compensates the load torque and the viscous damping. It has been proven that the selection of the nominal parameters for the DOB design has a restriction when they are too different from the real ones due to deterioration of the control system's stability [70]. Although the DOB compensates parameter variations between nominal and real parameters, we identified a discrepancy between the DOB and the real torque response of the motor when using the nominal parameters and a constant torque reference is applied. Therefore, we propose that in the implementation of the DOB, the experimental parameters should be used instead of the nominal parameters, resulting in equation (5).

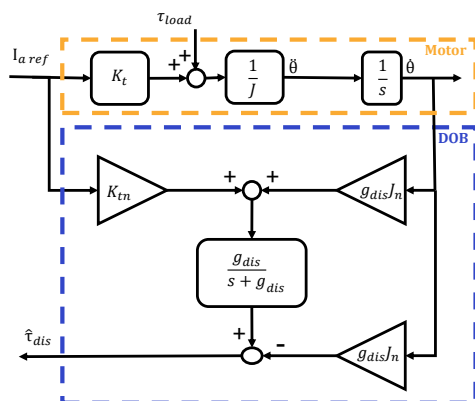


FIGURE 4. Disturbance observer block diagram.

$$\begin{bmatrix} K_{tn} \\ J_n \end{bmatrix} = \begin{bmatrix} K_t \\ J \end{bmatrix} \quad (5)$$

where K_{tn} is the nominal torque constant and J_n is the nominal inertia.

The experimental parameters were identified as follows: K_t as the inverse of the velocity constant K_v and J with equation (6).

$$J = \frac{T_m K_t K_e}{R_n} \quad (6)$$

where J is the inertia, K_e is the speed constant in V/rads, and R_n is the nominal armature resistance.

Before the final implementation, two calibrations were made to adjust the gains of the torque control. The two calibrations require the measurement of the real torque applied by the motor for comparison with the observed torque.

1) Open loop calibration

After defining the main elements of the DOB, an open loop calibration was made to adjust the gain, K_p , which is the control action. During this calibration the DOB response is monitored at open loop.

The open loop calibration involves measuring the real torque response applied by the motor with a dynamometer (force gauge) and a pulley of a known diameter (moment arm), as in Figure 5. Then the DOB response is monitored in an open loop, which should be ideally equal. After the measurement and monitoring, the error is calculated with equation (7).

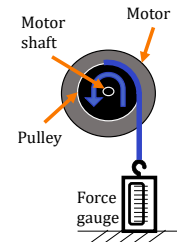


FIGURE 5. Force measuring for DOB in open loop calibration.

$$Err = \tau_{res} - \hat{\tau}_{dis} \quad (7)$$

where Err is the error, τ_{res} is the torque response measured, and $\hat{\tau}_{dis}$ is the observed disturbance torque (DOB response).

The DOB is implemented as feedback instead of a torque sensor; the performance of control in open loop is determined by the proportional gain, K_p , and the model of the plant. The proportional gain, typically called force control gain, C_f , determines how fast the control will try to lower the error to zero. The block diagram implemented for the open loop calibration is shown in Figure 6. Given a torque reference τ_{ref} , the control determines the armature current required to exert that torque reference based on a proportional gain and the factor J/K_t . A voltage gain, K_v , is added to the control, for

adjusting the voltage reference. The voltage reference is sent to the Pulse Width Modulation (PWM) generator to calibrate the voltage needed to obtain a certain torque reference τ_{ref} . For the first calibration, K_v is set to 1. To reduce Err , the first calibration was done after the experimental adjustments of the gain K_p .

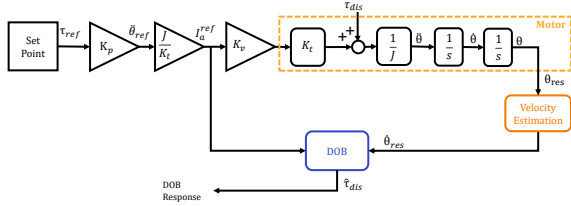


FIGURE 6. Block diagram for open loop calibration.

After the open loop calibration, the final implementation of the DOB is carried out in a closed loop control to compensate for the torque disturbances and possible parameter variations and to compute the error between the torque reference and the observed torque.

A pulley was attached to the motor shaft to pull a dynamometer to measure the torque τ applied by the motor with a 0.011 m moment arm. Simultaneously, the response of the DOB was monitored and saved by the controller to compare the torque τ_{dis} observed by the DOB. The parameters of Table 3 were considered.

TABLE 3. Parameters for the open loop calibration

Parameter	Description	Value
Set Point	Voltage reference	1.5 to 5.5V
K_t	Experimental torque constant	0.0605 Nm/A
J	Estimated rotor inertia	0.0004896 Kgm ²
g_{dis}	Cut-off frequency	500 rad/s
K_p	Proportional gain	1600
K_v	Proportional gain	1

The proportional gain K_p is adjusted to decrease the error between the torque measured at a constant voltage and the torque monitored from the DOB response. Figure 7 shows the torque response in open loop calibration. Both behaviors, the measured and observed torque, are linear as expected. In the plot, a linear regression is fitted and superimposed for each response to show the linearity. The similarity between the two responses matches the similarity of the fitted linear regressions. To decrease the error between the two responses, K_p is adjusted so the slopes are close. The measured response slope is 0.072 and the DOB monitoring slope is 0.051, which is close enough to reach the closed loop calibration.

2) Closed loop calibration

After adjusting the proportional gain K_p in the open loop calibration and monitoring the error in the DOB response, the second calibration in closed loop was carried out. This second calibration was made for monitoring the error response of the DOB and tune the voltage gain K_v . It is

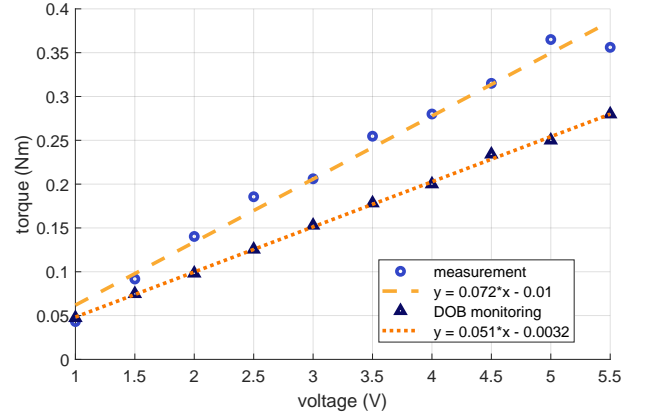


FIGURE 7. Torque response of torque control in open loop.

common to find regions of operation that can be identified by the increasing error in the DOB response. Therefore, the objective of the closed loop calibration was to reduce Err by determining the regions of operation. The block diagram implemented is shown in Figure 8.

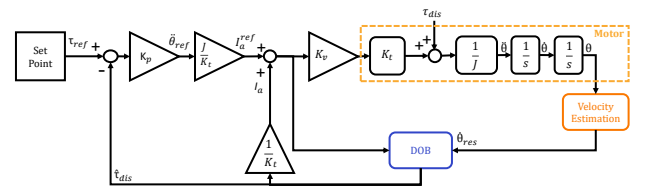


FIGURE 8. Closed loop control for second calibration.

Once the regions of operation are found, each region will have a voltage gain K_{vi} , where i is the number of regions. The final implementation of the DOB as a sensorless torque control is shown in Figure 9.

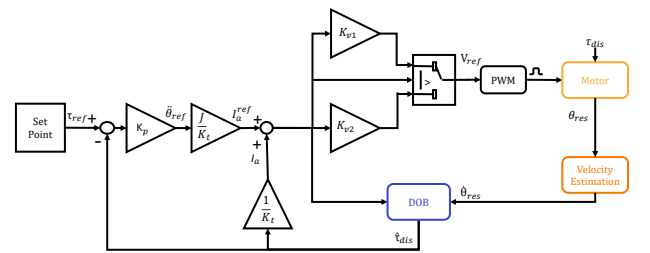


FIGURE 9. Final implementation of the DOB.

Figure 10 shows the plot of the torque applied by the motor (measured) and the torque of the DOB response, the comparison between this two data sets give us the error, Err .

The error is estimated as the difference between the measured torque applied and the DOB response after closing the loop with $K_p = 1600$ and $K_v = 1$. In the plot, two regions of operation are identified based on the error estimated for

each experiment. When the torque reference is larger than 0.15 Nm/A the error is positive, otherwise it is negative.

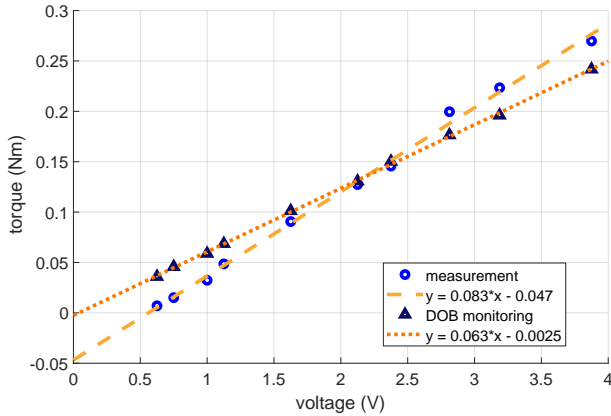


FIGURE 10. Torque response of torque control in closed loop.

To decrease the error, two K_v were proposed: K_{v_1} for the low torque region and K_{v_2} for the high torque region. In Table 4 the parameters used in the DOB-based torque control, after the open and closed loop calibrations, are shown.

TABLE 4. Final parameters of the torque control implemented

Parameter	Description	Value
Set Point	Torque reference	-0.5 to 0.5 Nm
K_t	Experimental torque constant	0.0605 Nm/A
J	Estimated rotor inertia	0.0004896 Kg m^2
g_{dis}	Cut-off frequency	500 rad/s
K_p	Proportional gain	1600
K_{v_1}	Proportional gain	1.25
K_{v_2}	Proportional gain	0.95

The final sensorless torque control implemented in the Haptic Lever is the one in Figure 9. The results at a step of 0.1 Nm, 0.2 Nm, and 0.3 Nm are shown in Figure 11. The system responded in every experiment at approximately 10 ms. A small vibration on the response, caused by the experimental setup, was observed. A cord was pulled to measure the torque exerted by the motor so the vibration could represent external disturbances.

The Haptic Lever could render torques from -0.5 Nm to 0.5 Nm due to the power source of 24 V and 7 A. The specifications of the rendered torques can be extended by using a larger power source, depending on the application. Since the objective of the Haptic Lever is to be used as a didactic tool for haptic augmentation in an SLE, the current torque specifications are sufficient.

IV. EXPERIMENTAL RESULTS OF THE HAPTIC AUGMENTATION TOWARDS AN SLE

Having the sensation of interacting with a virtual object through the sense of touch could increase the motivation and interest in learning about different physics topics related to force and torque interaction. The current learning environment can be enhanced with interactive tools that allow

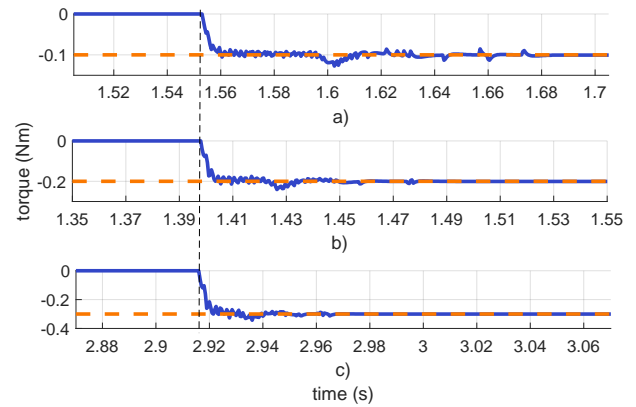


FIGURE 11. Torque control response at a step of a torque reference value in the Set Point. a) $\tau_{ref} = 0.1$ Nm, b) $\tau_{ref} = 0.2$ Nm, c) $\tau_{ref} = 0.3$ Nm.

students to feel and touch what they are calculating on paper or simulating in their computers. The Haptic Lever could be an alternative tool for bringing haptic augmentation to future learning environments. In this section, experiments related to constant, linear, and exponential force rendering are presented, by representing a virtual membrane, virtual springs, a virtual damper, and virtual point charges (Table 5). With these experiments, the functionality of the Haptic Lever, as a force display, is tested.

TABLE 5. Experiments of haptic augmentation towards a SLE

Force Behavior	Haptic Augmentation	Model
Constant	Membrane	$F = k_m$
Linear	Spring	$F = k_s x$
	Damper	$F = k_d \dot{x}$
Exponential	Point charge	$F = k_c / x^2$

In Figure 12 the main reference variables considered for the execution of the experiments are shown. The reference point marked as a circle will represent the different virtual objects. The lever, of length r , is manipulated by the user's hand. This way, the user can change the lever's position to get nearer or further from the reference point. The force that the user will feel during the interaction with the virtual object is F . This force, is the one rendered by the sensorless torque control, executed by the DC motor as a torque τ , and displayed on the lever. The reference variable x represents the distance between the reference position (virtual object) and the lever's current position, manually manipulated by the user.

The Haptic Lever can be used as a didactic tool to show students how a magnitude of force or torque feels. When students learn about abstract topics related to physical phenomena, it is common to simply do the numbers without thinking of how large or small a certain amount of force is. These four experiments presented in this paper are examples of the many applications that the Haptic Lever could represent with one DoF.

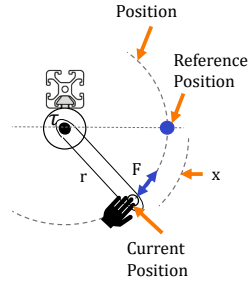


FIGURE 12. Reference variables of the haptic augmentation experiments.

A. CONSTANT FORCE BEHAVIOR (VIRTUAL MEMBRANE)

For the first experiment, a virtual membrane was programmed, as shown in Figure 13, with a constant force applied between two reference positions. When the Haptic Lever passes through the virtual membrane, the user feels an opposition to the motion. Once the Haptic Lever passes the virtual membrane, the user can manipulate the lever without restriction.

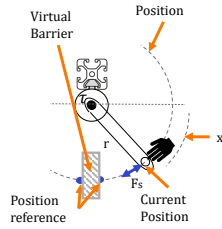


FIGURE 13. Virtual membrane experiment for constant force interaction.

This experiment could represent many applications. For example, if you think of the motor shaft as the pivot of a pair of scissors, the constant force could represent cutting a small string or passing through a membrane. The virtual membrane could also be rendered as an increasing or decreasing force as the user goes through the reference point

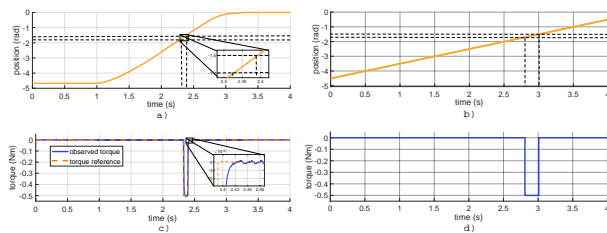


FIGURE 14. Simulation and experimental results for the experiment of passing through a virtual membrane. a) Experimental position when moving the Haptic Lever manually. b) Simulation of changing position at a constant velocity. c) Experimental results of the torque control response compared to the torque reference. d) Simulation of the torque response given a simulated change in position.

Figure 14 presents the experimental and simulation results of the interaction with a virtual membrane with constant

force. The reference points were defined in the positions 0.5 and 0.7 radians. Between these two points, the torque control applies a constant torque which is displayed through the lever as a constant force to the user. In the experimental results shown in Figure 14a, the user starts moving from approximately 4.5 radians towards the 0 radians position. As seen in Figure 14b, the experiment was performed while trying to move the lever at a constant velocity; the goal is to compare the results with the simulation. Along the way, as the user passes through the virtual membrane, the user senses a restriction to the motion before passing through. In Figure 14c, the constant force is applied between the reference points and the response to the torque reference step is shown in the change from -0.5 Nm to 0 Nm. The experimental results can be compared to the simulation results in Figure 14d in which the torque reference is an ideal step.

B. LINEAR FORCE BEHAVIOR (HOOKE'S LAW)

The Hooke's Law representation involves programming a virtual spring with a linear model. The force/torque reference is rendered in relation to the user's interaction with the virtual spring. Two experiments were developed, one for a compression spring and the second for a tension spring. The interaction force was estimated with Hooke's Law depicted in equation (8).

$$F_s = k_s x \quad (8)$$

where F_s is the interaction force, k_s is a known spring constant, and x is the compression/extension of the spring when F_s is applied at the end of the spring. The compression/extension is determined as the difference between a reference and current position of the Haptic Lever as shown in Figure 15. The force direction is represented in Figure 15a as an arrow that goes from the spring to the lever indicating the opposition force when the user contracts the spring. On the other hand, the force direction, in Figure 15b, is represented by an arrow that starts in the lever and goes to the spring indicating the tension exerted by the spring when the user extends it.

When the user interacts with the compression spring, the force increases in magnitude in the opposite direction to the motion of the hand as the user gets near to the reference position. With the tension spring, the reference point is located right on the side of the tension spring in a stationary state. When the user moves the lever away from the reference point, the force magnitude increases in opposition to the user's movement, pulling the hand of the user to the reference point. In both experiments, the torque applied by the motor is in opposite direction to the motion of the hand, rendering a dynamic force related to the user's interaction. The torque reference changes dynamically with the user's motion of the control and is proportional to the estimated force, F_r , as in equation (9).

$$\tau_{ref} = F_s r \quad (9)$$

where r is the moment arm of the Haptic Lever, $r = 0.1\text{m}$.

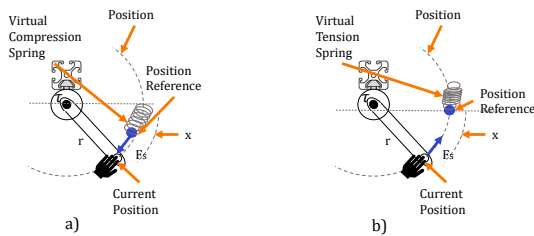


FIGURE 15. Linear force interaction with a virtual spring, a) References for compression spring, b) References for tension spring.

In Figure 16, the experimental and simulation results for the interaction with a compression spring are shown. The manual manipulation of the experimental results can be seen in Figure 16a. The lever’s position started around 3 radians, and after 1s, the lever was moved closer to the reference point in 0 radians. The virtual spring was touched in 0.5 radians to start the compression. From 0.5 to 0 radians the user kept moving, sensing a proportional increasing opposition force generated by the torque control, as shown in 16c. When the Haptic Lever reached the reference point of 0 radians, the force rendered shows that the compression spring is completely compressed so the maximum force of the spring is rendered. A small vibration in the torque displayed by the motor in the zoom area can be observed, and this may be caused by external disturbances related to the experimental setup. The behavior can be compared with the simulations of Figures 16b and 16d.

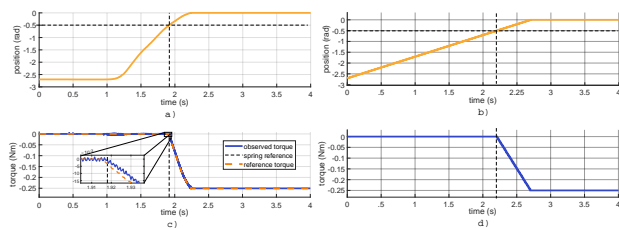


FIGURE 16. Simulation and experimental results for spring compression interaction experiment. a) Experimental position when moving the Haptic Lever manually. b) Simulation of changing position at a constant velocity. c) Experimental results of the torque control response compared to the torque reference. d) Simulation of the torque response given a simulated change in position.

In Figure 17 the experimental and simulation results of the interaction with a virtual tension spring are shown. The virtual tension spring is situated in a stationary state as shown Figure 15; the spring edge is in the 0 radians reference point. The experiment starts by pulling the spring from 0 radians to approximately 3 radians (Figure 17a). As in the previous experiments, the movement was made whilst trying to maintain a constant velocity to compare the behavior with the simulation in Figure 17b. As can be observed in Figure 17c, the maximum torque was reached at 1 radian, so the torque rendering is saturated at 0.5 Nm as a safety condition.

In the zoom area, a small vibration in the response was observed but the amplitude was not perceptible. The linear behavior of the torque rendering is similar to the simulation shown in Figure 17d.

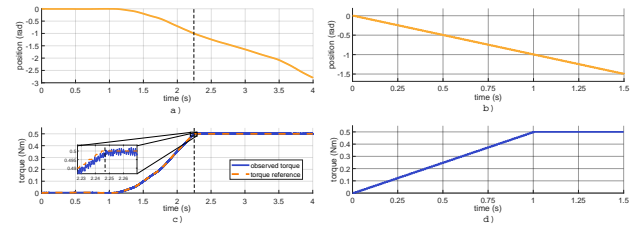


FIGURE 17. Simulation and experimental results for spring tension interaction experiment. a) Experimental position when moving the Haptic Lever manually. b) Simulation of changing position at a constant velocity. c) Experimental results of the torque control response compared to the torque reference. d) Simulation of the torque response given a simulated change in position.

C. LINEAR FORCE BEHAVIOR (DAMPER)

Linear force behavior can be represented in the form of a virtual damper following the viscous damping definition. The force exerted by the damper, when moving its rod, is directly proportional to the damping coefficient and the velocity of the motion as stated in equation 10.

$$F_d = k_d \dot{x} \quad (10)$$

where F_d is the interaction force, k_d is the damping coefficient, and \dot{x} is the velocity of the moving rod along the damper’s cylinder that in the case of the Haptic Lever it is an angular velocity.

The damping coefficient is characteristic of the virtual damper, the velocity is estimated with the N-method, described in a previous section. The virtual damper’s rod can be moved along the virtual damper’s cylinder as shown in Figure 18, where the position reference is at the beginning of the cylinder and the position indicates the stroke.

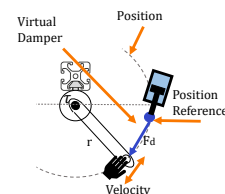


FIGURE 18. Linear force interaction with a virtual damper.

When the user interacts with the virtual damper, they move the Haptic Lever as if they move the virtual damper’s rod. If the motion is carried out with fast, the virtual rod is hard to move, but if the motion is slow, the virtual rod is moved with a low restriction. The motion can be done in two directions (from left to right). From that interaction, a torque reference is estimated with equation 11.

$$\tau_{ref} = F_d r \quad (11)$$

In Figure 19 the experimental results of the interaction with a virtual damper are depicted. Figure 19a shows the position during the manual manipulation, the virtual damper's rod starts moving at time 0.6s of the experiment. At this point, the rod is moved fast from 0 to 0.1 radians approximately. As it can be seen in Figure 19b the torque exerted by the Haptic Lever increases, up to 0.13 Nm, proportionally to the velocity of the motion shown in Figure 19c. The torque observed by the DOB, in Figure 19b, shows that the user feels the force behavior of a virtual damper since it follows the torque reference estimated with equation 11.

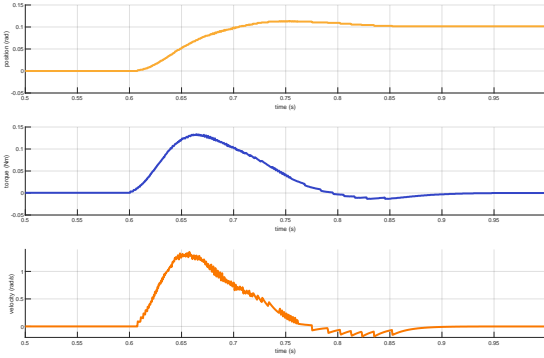


FIGURE 19. Manual interaction with a virtual damper. a) Position at manual manipulation of the Haptic Lever. b) Experimental results of the torque control response. c) Velocity measured during manual interaction.

D. EXPONENTIAL FORCE BEHAVIOR (COULOMB'S LAW)

Exponential forces were rendered in the form of electrostatic forces for the interaction between two virtual charges. The force magnitude exerted over a charged particle during the interaction with another one depends on the square distance between them and each one's charge value as can be observed in equation (12).

$$F_c = k \frac{q_1 q_2}{x^2} \quad (12)$$

where F_c is the electrostatic force, k is a proportional constant related to the nature of the medium in which the charges are situated, q_1 is the charge value of point charge 1, q_2 the charge value of point charge 2, and x is the distance between the two point charges. Since k , q_1 , and q_2 during the interaction of the two virtual charges are constant, they are taken as a single constant value k_c depicted in equation (13).

$$k_c = k q_1 q_2 \quad (13)$$

The force direction depends on the polarity of the virtual point charges. If they have different polarity, then they will be attracted. Otherwise, the force will represent repulsion between them. The torque reference τ_{ref} , is estimated with equation (14). In Figure 20, the reference positions of the virtual point charges are shown. The two-sided arrow represents

the electrostatic force in both directions since the force can be of attraction or repulsion depending on the experiment. The current position is a moving virtual point charge and the reference position is the location of a static point charge.

$$\tau_{ref} = F_m r \quad (14)$$

where F_m is the electrostatic force and r is the moment arm equivalent to the lever's length of 0.2 m.

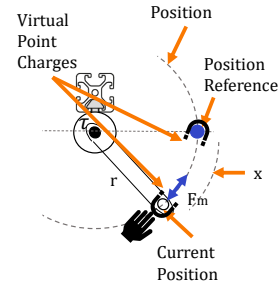


FIGURE 20. Virtual point charges experiment for electrostatic force attraction and repulsion interaction.

In Figure 21, the experimental and simulation results of the force rendering for the attraction with two virtual point charges are presented. In the experimental results of Figure 21a, the position of the lever was manipulated manually starting from 4.5 radians to 0 radians. During the experiment, the motion of the levers was as constant as possible to compare it to the simulation in Figure 21b where the position changes in a constant velocity. In the experimental results of Figure 21c, when the lever comes near the reference point, the magnitude of the torque increases exponentially in a positive direction giving the feeling of being attracted to the reference point in 0 radians. The experimental behavior is similar to the simulation presented in Figure 21d.

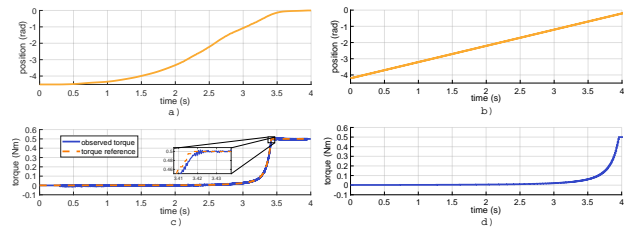


FIGURE 21. Simulation and experimental results for electrostatic attraction force interaction experiment. a) Experimental position when moving the Haptic Lever manually. b) Simulation of changing position at a constant velocity. c) Experimental results of the torque control response compared to the torque reference. d) Simulation of the torque response given a simulated change in position.

In Figure 22, the experimental results of the second experiment of Coulomb's Law are shown, where the repulsion force between two point charges is rendered. In the experimental results in Figure 22a, the motion starts, approximately, after 1.2 seconds. Since the starting position is 0 radians, the

starting torque applied by the motor is -0.5 Nm (maximum torque determined). The torque decreases exponentially in magnitude (Figure 22c) when the lever moves away from the reference position of the second point charge, at 0 radians. The user has the feeling of being repulsed from the reference point where the second point charge is situated. The position was simulated as a constant movement (Figure 22b) and the ideal force rendered can be seen in Figure 22d. The experimental results were similar to the simulation and follows the torque reference rendered. There are vibrations in the experimental results, but the amplitude is considered small for the didactic application.

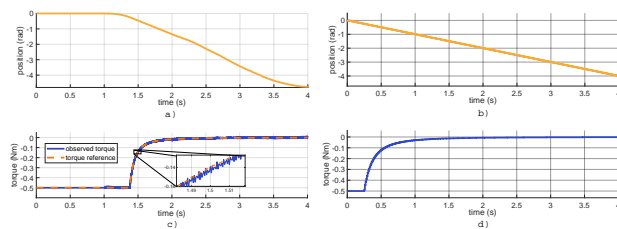


FIGURE 22. Simulation and experimental results for electrostatic repulsion force. a) Experimental position when moving the Haptic Lever manually. b) Simulation of changing position at a constant velocity. c) Experimental results of the torque control response compared to the torque reference. d) Simulation of the torque response given a simulated change in position.

E. DISCUSSION

After concluding the four experiments in which the Haptic Lever was used for interacting with virtual objects (membranes, springs, dampers and point charges), it was proven that the implementation of a DOB for a sensorless torque control allows the rendering of torques/forces following certain behavior. The DOB is a good alternative to PID-based controllers [59]. In this paper, the examples of haptic interaction were based on one DoF. The behaviors followed the model of four virtual objects.

Certainly, in the plots with the DOB design results, a small vibration can be observed. That vibration represents external disturbances, but their amplitude and frequency are not relevant for the didactic application objective. Then, the disturbances are not perceptible to the user so they can be neglected. The main objective was achieved since the Haptic Lever works as a haptic interface to display forces that represents the interaction with a membrane, a spring, and a point charge with constant, linear, and exponential behaviors, respectively. Commonly, the force/torque rendering is recommended to have a rate of at least 1 kHz for smooth behavior that allows a kinesthetic haptic device to have transparency [34]. The transparency indicates how real the artificial sense of touch feels; it is an important characteristic in all haptic devices, including teleoperation applications [63]. The Haptic Lever is considered to be transparent in terms of the control scheme response and force/torque rendering.

V. CONCLUSION

In this paper, a kinesthetic haptic interface, called the Haptic Lever, was presented for realistic haptic augmentation of force-related physical phenomena topics. The Haptic Lever was designed based on a sensorless torque control developed by means of a disturbance observer. The Haptic Lever was tested in four main experiments simulating haptic interaction with a virtual membrane, virtual springs and virtual point charges. The results obtained indicate an effective performance for rendering constant, linear, and exponential force/torque behavior.

The Haptic Lever design can be included in interactive technology designed for Smart Learning Environments. Although the Haptic Lever has not yet been implemented in courses, by observing the tests and results we believe the Haptic Lever could already be used in a classroom to introduce haptic augmentation in physics topics.

In further studies, the Haptic Lever will not only represent haptic augmentation but also visual augmentation, allowing the user to feel and see virtual objects in an AR environment. The specifications of the output torque of the system is limited due to the power source specifications. This limitation can be overcome by getting a power source with more output current.

It would be interesting to test the proposed design method of the Haptic Lever, to see engineering undergraduate students and teachers developing their own mock-ups of haptic interfaces. The possibility of representing the feeling of touch through a haptic device could increase the students interest in the development of new tools, methods, and control systems related to force feedback, which help to solve complex problems of interactions between a user and different environments, such as remote and virtual. Finally, there are many applications of custom-designed haptic interfaces like the Haptic Lever, including applications in medical training, medical assistance, rehabilitation, education assistance, industrial training, industrial assistance and entertainment. Depending on the application, the external disturbances can or cannot be neglected; therefore, for further work, the control of the Haptic Lever can be tuned, and the object modeling should be tested again.

ACKNOWLEDGMENT

The authors would like to thank the Universidad Autónoma de Ciudad Juárez (UACJ) for the support and equipment. This research was financially supported with funds from CONACYT, Ph.D. scholarship number 291197.

REFERENCES

- [1] C. Turkington and J. Harris, *The Encyclopedia of Memory and Memory Disorders*. 2nd ed., New York, NY, USA: Infobase Publishing, pp. 123, 2002.
- [2] J. Dron, "Smart learning environments, and not so smart learning environments: A systems view," *Smart Learning Environments*, vol. 5, no. 25, pp. 1–20, 2018.
- [3] K. Duncan, *The diagrams book: 50 ways to solve any problem visually*, London, UK: LID Publishing, 2013.

- [4] J. Bernhard, "What matters for students' learning in the laboratory? Do not neglect the role of experimental equipment," *Instructional Science*, vol. 46, no. 6, pp. 819–846, 2018.
- [5] L. Chamba-Eras and J. Aguilar, "Augmented reality in a smart classroom-case study: SaCI," *IEEE Revista Iberoamericana de Tecnologías del Aprendizaje*, vol. 12, no. 4, pp. 165–172, 2017.
- [6] B. Edwards, K. Bielawski, R. Prada, and A. Cheok, "Haptic virtual reality and immersive learning for enhanced organic chemistry instruction," *Virtual Reality*, pp. 1–11, 2018.
- [7] A. Okamura, C. Rochard, and M. Cutkosky, "Feeling is believing: Using a force-feedback joystick to teach dynamic systems," *Journal of Engineering Education*, vol. 91, no. 3, pp. 345–349, 2002.
- [8] C. Rose, C. McDonald, J. Clark, and M. O' Malley, "Reflection on system dynamics principles improves student performance in haptic paddle labs," *IEEE Transactions on Education*, vol. 61, no. 3, pp. 245–252, 2018.
- [9] R. Gassert, J. Metzger, K. Leuenberger, W. Popp, M. Tucker, B. Vigar, R. Zimmermann, and O. Lamberg, "Physical student-robot interaction with the ETHZ haptic paddle," *IEEE Transactions on Education*, vol. 56, no. 1, pp. 9–17, 2013.
- [10] U. Shaikh, A. Magana, L. Neri, D. Escobar-Castillejos, J. Noguez, and B. Benes, "Undergraduate students' conceptual interpretation and perceptions of haptic-enabled learning experiences," *International Journal of Educational Technology in Higher Education*, vol. 14, no. 15, pp. 1–21, 2017.
- [11] K. Murphy, and M. Darrah, "Haptics-based apps for middle school students with visual impairments," *IEEE Transactions on Haptics*, vol. 8, no. 3, pp. 318–326, 2015.
- [12] H. Lee, G. Han, I. Lee, S. Yim, K. Hong, H. Lee, and S. Choi, "Haptic assistance for memorization of 2-D selection sequences," *IEEE Transactions on Human-Machine Systems*, vol. 43, no. 6, pp. 643–649, 2013.
- [13] P. Carlson, A. Peters, S. Gilbert, J. Vance, and A. Luse, "Virtual training: Learning transfer of assembly tasks," *IEEE Transactions on Human-Machine Systems*, vol. 43, no. 6, pp. 643–649, 2013.
- [14] S. Jeon and M. Harders, "Haptic tumor augmentation: Exploring multi-point interaction," *IEEE Transactions on Haptics*, vol. 7, no. 4, pp. 477–485, 2014.
- [15] N. Najmaei, A. Asadian, M. Kermani, and R. Patel, "Design and Performance Evaluation of a Prototype MRF-Based Haptic Interface for Medical Applications," *IEEE/ASME Transactions on Mechatronics*, vol. 21, no. 1, pp. 110–121, 2016.
- [16] B. Schneider and P. Blikstein, "Flipping the flipped classroom: A study of the effectiveness of video lectures versus constructivist exploration using tangible user interfaces," *IEEE Transactions on Learning Technologies*, vol. 9, no. 1, pp. 5–17, 2016.
- [17] P. Punpongson, D. Iwai, and K. Sato, "SoftAR: Visually manipulating haptic softness perception in spatial augmented reality," *IEEE Transactions on Visualization and Computer Graphics*, vol. 21, no. 11, pp. 1279–1288, 2015.
- [18] Y. Lin, "Impacts of a flipped classroom with a smart learning diagnosis system on students' learning performance, perception, and problem solving ability in a software engineering course," *Computers in Human Behavior*, vol. 95, pp. 187–196, 2019.
- [19] Y. Kim, T. Soyata, and R. Behnagh, "Towards emotionally aware AI smart classroom: Current issues and directions for engineering and education," *IEEE Access*, vol. 6, pp. 5308–5331, 2018.
- [20] M. Muñoz-Organero, P. Muñoz-Merino, and C. Delgado-Kloos, "Personalized service-oriented E-Learning environments," *IEEE Internet Computing*, vol. 11, no. 2, pp. 62–67, 2010.
- [21] C. Hung, F. O. Kuo, J. Sun, and P. Yu, "An interactive game approach for improving students' learning performance in multi-touch game-based learning," *IEEE Transactions on Learning Technologies*, vol. 7, no. 1, pp. 31–37, 2014.
- [22] M. Javaid, S. Ashrafi, M. Žefran, and A. Steinberg, "ToothPIC: An interactive application for teaching oral anatomy," *IEEE Transactions on Learning Technologies*, vol. 9, no. 2, pp. 184–189, 2016.
- [23] X. Wei, D. Weng, Y. Liu, and Y. Wang, "Teaching based on augmented reality for a technical creative design course," *Computers and Education*, vol. 81, pp. 221–234, 2015.
- [24] International Association of Smart Learning Environments. *Smart Learning*, Accessed: Jan. 2019. [Online]. Available: <http://iasle.net/about-us/background/>.
- [25] R. Koper, "Conditions for effective smart learning environments," *Smart Learning Environments*, vol. 1, no. 5, pp. 1–17, 2014.
- [26] Y. Kim, S. Jeong, Y. Ji, S. Lee, K. Kwon, and J. Jeon, "Smartphone response system using twitter to enable effective interaction and improve engagement in large classrooms," *IEEE Transactions on Education*, vol. 58, no. 2, pp. 98–103, 2015.
- [27] J. Yang, H. Pan, W. Zhou, and R. Huang, "Evaluation of smart classroom from the perspective of infusing technology into pedagogy," *Smart Learning Environments*, vol. 5, no. 20, pp. 1–11, 2018.
- [28] T. Hoel and J. Mason, "Standards for smart education – towards a development framework," *Smart Learning Environments*, vol. 5, no. 3, pp. 1–25, 2018.
- [29] C. Wang, X. Li, A. Wang, and X. Zhou, "A classroom scheduling service for smart classes," *IEEE Transactions on Services Computing*, vol. 10, no. 2, pp. 155–164, 2017.
- [30] J. Minogue and M. Jones, "Haptics in education: Exploring an untapped sensory modality," *Review of Educational Research*, vol. 76, no. 3, pp. 317–348, 2006.
- [31] Nicolas Herzig and Perla Maiolino and Fumiya Iida and Thirishantha Nanayakkara, "A Variable Stiffness Robotic Probe for Soft Tissue Palpation," *IEEE Robotics and Automation Letters*, vol. 3, no. 2, pp. 1168–1175, 2018.
- [32] Hunor Erdelyi and Doru Talaba, "Virtual prototyping of a car turn-signal switch using haptic feedback," *Engineering with Computers*, vol. 26, no. 1, pp. 99–110, 2010.
- [33] Aleš Hacı and Mitja Golob, "Chattering-free Sliding Mode Control Algorithm for a Haptic Throttle Lever," *IECON 2016 - 42nd Annual Conference of the IEEE Industrial Electronics Society*, Florence, 2016, pp. 6385–6390.
- [34] G. Robles-De-La-Torre, "The importance of the sense of touch in virtual and real environments," *IEEE MultiMedia*, vol. 13, no. 3, pp. 24–30, 2006.
- [35] E. Whitmire, H. Benko, C. Holz, E. Ofek, and M. Sinclair, "Haptic revolver: Touch, shear, texture, and shape rendering on a reconfigurable virtual reality controller," *Conference on Human Factors in Computing Systems (CHI Honourable Mention)*, 2018, pp. 1–12.
- [36] B. Son and J. Park, "Haptic feedback to the palm and fingers for improved tactile perception of large objects," *Proceedings of the 31st Annual ACM Symposium on User Interface Software and Technology (UIST)*, 2018, pp. 757–763.
- [37] F. Chinello, M. Malvezzi, D. Prattichizzo, and C. Pacchierotti, "A modular wearable finger interface for cutaneous and kinesthetic interaction: Control and evaluation," *IEEE Transactions on Industrial Electronics*, vol. 67, no. 1, pp. 706–716, 2020.
- [38] J. Lee, M. Sinclair, M. Gonzalez-franco, E. Ofek, and C. Holz, "TORC: A virtual reality controller for in-hand high-dexterity finger interaction," *Conference on Human Factors in Computing Systems (CHI)*, 2019, pp. 1–13.
- [39] E. Scilingo, M. Bianchi, G. Grioli, and A. Bicchi, "Rendering Softness: Integration of Kinesthetic and Cutaneous Information in a Haptic Device," *IEEE Transactions on Haptics*, vol. 3, no. 2, pp. 109–118, 2010.
- [40] C. Pacchierotti, A. Tirmizi, G. Bianchini, and D. Prattichizzo, "Enhancing the Performance of Passive Teleoperation Systems via Cutaneous Feedback," *IEEE Transactions on Haptics*, vol. 8, no. 4, pp. 397–409, 2015.
- [41] J. Park, Y. Oh, and H. Tan, "Effect of Cutaneous Feedback on the Perceived Hardness of a Virtual Object," *IEEE Transactions on Haptics*, vol. 11, no. 4, pp. 518–530, 2018.
- [42] H. Kim, H. Yi, H. Lee, and W. Lee, Woohun, "HapCube: A wearable tactile device to provide tangential and normal pseudo-force feedback on a fingertip," *Conference on Human Factors in Computing Systems (CHI Honourable Mention)*, 2018, pp. 1–13.
- [43] G. Park, H. Cha, and S. Choi, "Haptic Enchanters: Attachable and Detachable Vibrotactile Modules and Their Advantages," *IEEE Transactions on Haptics*, vol. 12, no. 1, pp. 43–55, 2019.
- [44] G. García-Valle, M. Ferre, J. Breñosa, and D. Vargas, "Evaluation of presence in virtual environments: Haptic vest and user's haptic skills," *IEEE Access*, vol. 6, pp. 7224–7233, 2018.
- [45] F. Chinello, C. Pacchierotti, J. Bimbo, N. Tsagarakis, and D. Prattichizzo, "Design and Evaluation of a Wearable Skin Stretch Device for Haptic Guidance," *IEEE Robotics and Automation Letters*, vol. 3, no. 1, pp. 524–531, 2018.
- [46] H. Culbertson, J. Walker, M. Raitor, A. Okamura, "WAVES: A Wearable Asymmetric Vibration Excitation System for Presenting Three-Dimensional Translation and Rotation Cues," *Conference on Human Factors in Computing Systems (CHI)*, 2017, pp. 4972–4982.
- [47] Q. Tong, Z. Yuan, X. Liao, M. Zheng, T. Yuan, and J. Zhao, "Magnetic levitation haptic augmentation for virtual tissue stiffness perception," *IEEE*

- Transactions on Visualization and Computer Graphics*, vol. 24, no. 12, pp. 3123–3136, 2018.
- [48] D. Grajewski, and F. Górski, and A. Hamrol, “Immersive and haptic educational simulations of assembly workplace conditions,” *2015 International Conference on Virtual and Augmented Reality in Education (VARE)*, 2015, pp. 359–368.
- [49] C. Rose, J. French, and M. O’Malley, “Design and characterization of a haptic paddle for dynamics education,” *IEEE Haptics Symposium 2014*, 2014, pp. 265–270.
- [50] C. Rose, C. McDonald, J. Clark, and M. O’Malley, “Reflection on System Dynamics Principles Improves Student Performance in Haptic Paddle Labs,” *IEEE Transactions on Education*, vol. 61, no. 3, pp. 245–252, 2018.
- [51] C. Tadiello, G. De Rossi, M. Capiluppi, R. Muradore, and P. Fiorini, “Teaching physical human-robot interaction to computer science undergraduate students,” *2016 European Control Conference (ECC)*, 2016, pp. 376–381.
- [52] I. Choi, E. Ofek, H. Benko, M. Sinclair, and C. Holz, “CLAW: A multifunctional handheld haptic controller for grasping, touching, and triggering in virtual reality,” *Conference on Human Factors in Computing Systems (CHI)*, 2018, pp. 1–13.
- [53] Y. Zhao, C. Bennett, H. Benko, E. Cutrell, C. Holz, M. Morris, and M. Sinclair, “Enabling people with visual impairments to navigate virtual reality with a haptic and auditory cane simulation,” *Conference on Human Factors in Computing Systems (CHI)*, 2018, pp. 1–14.
- [54] E. Strasnick, C. Holz, E. Ofek, M. Sinclair, and H. Benko, “Haptic links: Bimanual haptics for virtual reality using variable stiffness actuation,” *Conference on Human Factors in Computing Systems (CHI)*, 2018, pp. 1–14.
- [55] T. Ando, R. Tsukahara, M. Seki, and M. G. Fujie, “A haptic interface “Force Blinker 2” for navigation of the visually impaired,” *IEEE Transactions on Industrial Electronics*, vol. 59, no. 11, pp.4112–4119, 2012.
- [56] R. Lee, R. Klatzky, and G. Stetten, “In-situ force augmentation improves surface contact and force control,” *IEEE Transactions on Haptics*, vol. 10, no. 4, pp. 545–554, 2017.
- [57] E. Sariyildiz and K. Ohnishi, “On the explicit robust force control via disturbance observer,” *IEEE Transactions on Industrial Electronics*, vol. 62, no. 3, pp. 1581–1589, 2015.
- [58] E. Sariyildiz and K. Ohnishi, “An adaptive reaction force observer design,” *IEEE/ASME Transactions on Mechatronics*, vol. 20, no. 2, pp. 750–759, 2015.
- [59] R. Oboe, “How disturbance observer changed my life,” *IEEE 15th International Workshop on Advanced Motion Control (AMC)*, 2018, pp. 13–20.
- [60] F. Lin, Y. Hung, and S. Chen, “FPGA-based computed force control system using Elman neural network for linear ultrasonic motor,” *IEEE Transactions on Industrial Electronics*, vol. 56, no. 4, pp. 1238–1253, 2009.
- [61] H. Tanaka, K. Ohnishi, H. Nishi, T. Kawai, Y. Morikawa, S. Ozawa, and T. Furukawa, “Implementation of bilateral control system based on acceleration control using FPGA for multi-DOF haptic endoscopic surgery robot,” *IEEE Transactions on Industrial Electronics*, vol. 56, no. 3, pp. 618–627, 2009.
- [62] E. Ishii, H. Nishi, and K. Ohnishi, “Improvement of performances in bilateral teleoperation by using FPGA,” *IEEE Transactions on Industrial Electronics*, vol. 54, no. 4, pp. 1876–1884, 2007.
- [63] Zheng Chen and Fanghao Huang and Chunling Yang and Bin Yao, “Adaptive Fuzzy Backstepping Control for Stable Nonlinear Bilateral Teleoperation Manipulators With Enhanced Transparency Performance,” *IEEE Transactions on Industrial Electronics*, vol. 67, no. 1, pp. 746–756, 2020.
- [64] M. Nandayapa, C. Mitsantisuk, and K. Ohishi, “Velocity control based on a wide range of velocity estimation in FPGA,” *IEEJ/Japan Conference on Industrial Instrumentation and Control*, 2011, pp. 89–94.
- [65] M. Nandayapa, C. Mitsantisuk, and K. Ohishi, “Improving bilateral control feedback by using novel velocity and acceleration estimation methods in FPGA,” *The 12th IEEE International Workshop on Advanced Motion Control*, 2012, pp. 1–6.
- [66] K. Ohishi, K. Ohnishi, and K. Miyachi, “Torque-speed regulation of a DC motor based on load torque estimation method,” *International Power Electronics Conference (IEEJ)*, 1983, pp. 1209–1218.
- [67] A. Hace and M. Franc, “Pseudo-Sensorless High-Performance Bilateral Teleoperation by Sliding-Mode Control and FPGA,” *IEEE/ASME Transactions on Mechatronics*, vol. 19, no. 1, pp. 384–393, 2014.
- [68] E. Sariyildiz, R. Oboe, and K. Ohnishi, “Disturbance Observer-based Robust Control and Its Applications: 35th Anniversary Overview,” *IEEE Transactions on Industrial Electronics*, vol. 67, no. 3, pp. 2042–2053, 2020.
- [69] W. Chen, J. Yang, L. Guo, and S. Li, “Disturbance-Observer-Based Control and Related Methods—An Overview,” *IEEE Transactions on Industrial Electronics*, vol. 63, no. 2, pp. 1083–1095, 2016.
- [70] H. Kobayashi, S. Katsura, and K. Ohnishi, “An Analysis of Parameter Variations of Disturbance Observer for Motion Control,” *IEEE Transactions on Industrial Electronics*, vol. 54, no. 6, pp. 3413–3421, 2007.

...